Nonequilibrium steady states in a closed inhomogeneous asymmetric exclusion process with generic particle nonconservation

Bijoy Daga,[1,*] Souvik Mondal,[1,†] Anjan Kumar Chandra,[2,‡] Tirthankar Banerjee,[1,§] and Abhik Basu[1,‖]
[1]*Condensed Matter Physics Division, Saha Institute of Nuclear Physics, Calcutta 700064, India*
[2]*Department of Physics, Malda College, Malda, West Bengal 732101, India*
(Received 27 September 2016; published 9 January 2017)

We study the totally asymmetric exclusion process (TASEP) on a nonuniform one-dimensional ring consisting of two segments having unequal hopping rates, or *defects*. We allow weak particle nonconservation via Langmuir kinetics (LK), which are parametrized by generic unequal attachment and detachment rates. For an extended defect, in the thermodynamic limit the system generically displays inhomogeneous density profiles in the steady state—the faster segment is either in a phase with spatially varying density having no density discontinuity, or a phase with a discontinuous density changes. Nonequilibrium phase transitions between the above phases are controlled by the inhomogeneity and LK. The slower segment displays only macroscopically uniform bulk density profiles in the steady states, reminiscent of the maximal current phase of TASEP but with a bulk density generally different from half. With a point defect, there are spatially uniform low- and high-density phases as well, in addition to the inhomogeneous density profiles observed for an extended defect. In all the cases, it is argued that the mean particle density in the steady state is controlled only by the ratio of the LK attachment and detachment rates.

DOI: 10.1103/PhysRevE.95.012113

I. INTRODUCTION

The effects of nonuniformities or disorders on the macroscopic properties of equilibrium systems are well understood by now within the general framework of statistical mechanics [1]. In contrast, the effects of quenched disorders on the dynamics and nonequilibrium steady states (NESS) of out-of-equilibrium systems are much less understood [2]. The totally asymmetric simple exclusion process (TASEP) and its variants with open boundaries in one dimension serve as simple models of restricted one-dimensional (1D) transport [3]. Natural realizations of TASEP include motions in a nuclear pore complex of cells [4], motion of molecular motors along microtubules [5], fluid flow in artificial crystalline zeolites [6], and protein synthesis by a messenger RNA (mRNA) ribosome complex in cells [7]; see, e.g., Refs. [3] for basic reviews on asymmetric exclusion processes. Subsequently, studies on TASEP with particle nonconservation in the form of on-off Langmuir kinetics (LK) [8] in the limit when LK competes with the hopping movement of TASEP reveal an unusual phase coexistence in the NESS, not found in pure TASEP. Furthermore, open TASEPs with defects [9], both point and extended, have been studied, which investigated the effects of the defects on the NESS and currents. The open TASEP with a single point defect along with LK is shown to display a variety of phases and phase coexistence as a result of the competition between the defect and LK [10].

Studies of TASEP in a closed ring are relatively few and far between. Translational invariance ensures that TASEP in a homogeneous ring, with or without LK produces a homogeneous density profile in the steady state. Nonuniform or inhomogeneous steady states are expected only with explicit breakdown of the translation invariance, e.g., by means of quench disorder in the hopping rates at different sites. Exclusion processes in closed inhomogeneous rings with strict particle number conservation have been shown to display inhomogeneous NESS [11–13]. More recently, TASEP in a ring with quench disordered hopping rates together with nonconserving LK having equal rates of particle attachment and detachment has been studied in Ref. [14]. Quite unexpectedly, the model admits only macroscopically inhomogeneous NESS, in the forms of two- and three-phase coexistence, regardless of extended or point defects, a feature that has been explained in general terms in Ref. [14]. Equal attachment and detachment rates, as used in Ref. [14], are actually an idealization and simplification. In typical physical realizations of this model, e.g., vehicular/pedestrian traffic and ribosome translocations along closed mRNA loops in the presence of defects with particle nonconservation, attachment and detachment rates are generically expected to be unequal. This calls for studies to find how unequal rates will affect the results of Ref. [14], or the robustness of the results in Ref. [14] against variation in the ratio K of the attachment and detachment rates. In this work, we set out to study this question by considering TASEP in a two-segment ring having unequal hopping rates with LK. How LK dynamics with $K \neq 1$ affects the phases of an open TASEP is studied in Ref. [8]. Here, we analyze how the interplay of LK with $K \neq 1$ and quenched inhomogeneity affects the NESS of a TASEP on a ring. The latter admits only strictly uniform density due to the particle number conservation and translational invariance, and it has no phase transitions. In the present study, we find that with an extended defect, in the NESS the faster segment displays either an inhomogeneous (spatially nonuniform) phase with *no discontinuity* in the density (hereafter a *continuous density phase*, or CDP) and a phase with a discontinuous change or a shock (hereafter a *shock phase*, or SP) in the density profile for all values of

*bijoy.daga@saha.ac.in
†souvik.mondal@saha.ac.in
‡anjanphys@gmail.com
§tirthankar.banerjee@saha.ac.in
‖abhik.basu@saha.ac.in;abhik.123@gmail.com

the defect strength (i.e., the hopping rate along the extended defect) and the ratio of the attachment and detachment rates. Steady-state density profiles in the CDP are found to have three parts—two parts with nonzero spatial gradients of the density, and an intervening part having a constant magnitude of $n_0 = K/(1+K)$, i.e., with zero slope. In general, $n_0 \neq 1/2$ for $K \neq 1$, unlike the corresponding result in Ref. [14]. The CDP and SP, respectively, are the direct generalizations of the three- and two-phase coexistence for $K = 1$ [14]. By tuning the model parameters, nonequilibrium transitions between CDP and SP are observed. The steady-state density in the slower segment is *always* macroscopically uniform. Being controlled solely by the LK attachment and detachment rates, the value of the steady-state density in the slower segment is n_0. This is reminiscent of the maximal current (MC) phase of TASEP, but with a current generically less than $1/4$ for $K \neq 1$. In contrast, for a point defect, the model can display spatially macroscopically uniform steady states for either K very small or very large, yielding either low-density (LD) or high-density (HD) phases. For intermediate values of K, the model exhibits nonuniform phases—either CDP or SP, as with an extended defect. Nonequilibrium transitions between all three types of phases are again controlled by the LK attachment-detachment rates and inhomogeneity. Lastly, in all the phases of both extended and point defects, the mean particle density in the NESS of the system is argued to be n_0, i.e., controlled only by K. Our study is a close-ring analog of the model in Ref. [8] that considered an open system. Our results, as described in detail below, manifestly reveal the significance of the ring geometry in controlling NESS. The rest of the article is organized as follows: In Sec. II, we define our model. Then, a short review of the results for $K = 1$ is presented in Sec. II A. In Secs. III A and III B, we analyze the NESS of the model with an extended and a point defect, respectively. A brief comparison of the results in the present work with the corresponding results for $K = 1$ is made in Sec. IV. We summarize in Sec. V at the end of the paper.

II. THE MODEL

Consider a TASEP of N sites together with LK on a 1D periodic ring with spatial inhomogeneity. Due to exclusion, the particle occupation n_i at each site i is either 0 or 1. In TASEP, a particle can only hop to its immediate vacant neighbor in one direction, say anticlockwise (see Fig. 1). Spatial inhomogeneity in the model is then introduced by unequal hopping rates of the particles in the two segments, one faster and the other slower, marked CHI and CHII, respectively, in Fig. 1. The hopping rates in CHI and CHII, respectively, are 1 and $p(<1)$. Let N_1 and N_2 be the respective sizes of CHI and CHII, such that $N_1 + N_2 = N$. We define $l = N_1/N$ as the fraction of the total sites in CHI; $N_1 = Nl$, $N_2 = (1-l)N$. Note that since the hopping rates do not evolve in time, the spatial inhomogeneities considered here are quenched. Further, due to LK, a particle can detach from a given site with rate ω or attach to a given site with rate ωK. We work in the regime where TASEP competes with LK dynamics, such that the net flux due to TASEP must be comparable to the total flux due to LK. To ensure this, we apply the scaling relations $\Omega = \omega N$, where N is a large but finite number, and we study

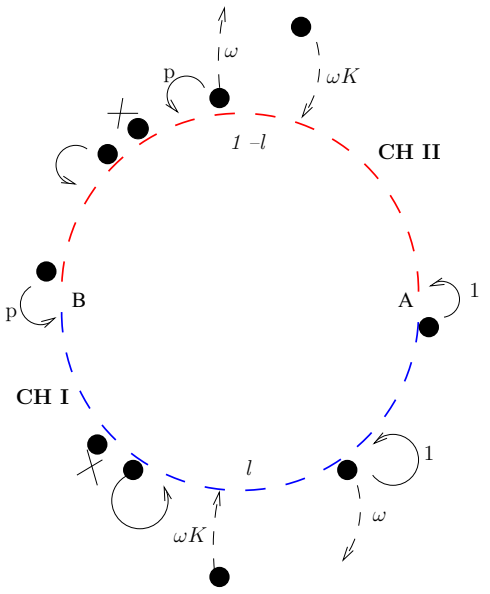

FIG. 1. TASEP and LK dynamics on a 1D ring with unequal hopping rates in CHI and CHII; the LK detachment and attachment rates are ω and ωK, respectively; see the text.

the system in the limit $\Omega \sim O(1)$ [8,14]. For convenience, we label the sites by a continuous variable x in the thermodynamic limit, defined by $x = i/N, 0 < x < 1$. In terms of the rescaled coordinate x, the lengths of CHI and CHII are l and $1-l$, respectively. The coordinate x rises from junction B ($x = 0$) to junction A ($x = l$) in the anticlockwise direction.

A. Short review of the results for $K = 1$

We briefly review the results for $K = 1$ [14], i.e., with equal attachment and detachment rates. The mean-field (MF) equations are set up in both CHI and CHII. The steady-state densities are then calculated by observing that current is conserved *locally*, and hence current conservation can be applied very close to junctions A and B:

$$n_{\rm I}(y)[1-n_{\rm I}(y)] = p n_{\rm II}(y)[1-n_{\rm II}(y)], \tag{1}$$

where $y =$ junction A or B. The steady-state densities are given by

$$n_{\rm IB}(x) = \Omega x + \frac{1-\sqrt{1-p}}{2}, \tag{2}$$

$$n_{\rm IA}(x) = \Omega(x-l) + \frac{1+\sqrt{1-p}}{2}, \tag{3}$$

such that both Eqs. (2) and (3) depend upon the density values at junctions B and A, respectively. In contrast,

$$n_{\rm Ib}(x) = \tfrac{1}{2} \tag{4}$$

and

$$n_{\rm II}(x) = \tfrac{1}{2} \tag{5}$$

are the *bulk* solutions independent of the densities at the junctions, and they are an analog of the MC phase in an open TASEP. In CHI, let x_α and x_β, respectively, be the points where

the left solution $n_{\rm IB}(x)$ and the right solution $n_{\rm IA}(x)$ meet with the bulk solution $n_{\rm Ib}$. It was shown that

$$x_\beta - x_\alpha = l - \frac{\sqrt{1-p}}{\Omega}. \tag{6}$$

Thus if $x_\alpha < x_\beta$, the system is in a three-phase (LD-MC-HD) coexistence. But if $x_\alpha > x_\beta$, the system can be only in a two-phase (LD-HD) coexistence. The critical line separating the two phases can thus be determined by setting $x_\alpha = x_\beta$. Further, the global average density of the system is always $n_0 = 1/2$, irrespective of the chosen values of p and Ω.

III. STEADY-STATE DENSITIES

We perform MF analysis of our model, supplemented by extensive Monte Carlo simulations (MCS). We present our results for an extended and a point defect separately below. We consider only $K < 1$; the results for $K > 1$ may be obtained from those for $K < 1$ together with the particle-hole symmetry. In our MCS studies, we use a random-sequential update scheme. We measure the average site density $\langle n_i \rangle$ over approximately 2×10^9 Monte Carlo steps after relaxing the system for 10^9 Monte Carlo steps. We separately study an extended and a point defect. For an extended defect here, $0 < l < 1$, whereas for a point defect, $l \to 1$. In Ref. [8], the authors solved the steady-state densities in the analogous open system in terms of the Lambert W functions. Here, we use the implicit solutions of the densities in the steady state, which suffice for our purposes.

A. MF analysis and MCS results for an extended defect

We set up our MF analysis by closely following the logic outlined in Ref. [14]. In our MF analysis, we describe the model as a combination of two TASEPs—CHI and CHII—joined with each other at the junctions A and B; see Fig. 1. Thus, junctions B and A are *effective* entry (exit) and exit (entry) ends of CHI (CHII). This allows us to analyze the phases of the system in terms of the known phases of the open-boundary LK-TASEP [8]. Without LK, the steady-state densities of a TASEP in an inhomogeneous ring are completely determined by the total particle number (a conserved quantity) in the system in the steady state and the inhomogeneity configurations [11–13]. Due to the nonconserving LK dynamics, however, the particle current here is conserved only *locally*, since the probability of attachment or detachment at a particular site vanishes as $1/N$ [8,14]. Hence, the total particle number in the NESS is not a conserved quantity. The steady-state densities $n_{\rm I}(x)$ and $n_{\rm II}(x)$ in CHI and CHII, respectively, follow [8,14]

$$[2n_{\rm I}(x) - 1]\frac{\partial n_{\rm I}(x)}{\partial x} - \Omega(1+K)\left(n_{\rm I}(x) - \frac{K}{1+K}\right) = 0 \tag{7}$$

and

$$p[2n_{\rm II}(x) - 1]\frac{\partial n_{\rm II}(x)}{\partial x} - \Omega(1+K)\left(n_{\rm II}(x) - \frac{K}{1+K}\right) = 0. \tag{8}$$

Before we attempt to solve Eqs. (7) and (8), we define an average density n_0 in a given NESS that remains a constant on average, although the model dynamics does not admit any conservation law for the total particle number. In the homogeneous limit of the model, i.e., with $p = 1$, CHI and CHII are identical and the steady-state density is spatially uniform, due to the translational invariance for $p = 1$ for all K. Equation (7) or (8) then yields

$$n_0 = \frac{K}{K+1}. \tag{9}$$

Thus, the average hole density is $1 - n_0$ for $p = 1$. A global deviation of the mean density from n_0 should indicate either more particles or more holes entering into the system in the steady state than that given by n_0. However, even when inhomogeneity is introduced ($p < 1$), there is nothing that favors either particles or holes, since the inhomogeneity that acts as an inhibitor for the particle current acts equally as an inhibitor for the hole current. Hence, it is not expected to affect the value of n_0. This forms a major result of this work that is in agreement with the MCS studies; see below. Notice that this argument does not preclude any local excess of particles or holes, since the particles and the holes move in opposite directions, and hence the presence of a defect should lead to excess particles on one side and excess holes (equivalently deficit particles) on the other. This holds for any Ω and K. When $K = 1$, $n_0 = 1/2$, in agreement with Ref. [14]. Equations (7) and (8) are first-order differential equations, each having one constant of integration in their solutions. These may be determined by considering the current conservation or "boundary conditions" at junctions A and B. In addition, Eqs. (7) and (8) admit a third spatially constant solution independent of the boundaries, given by $K/(1+K)$. Since CHI has a higher hopping rate ($1 > p$), on physical grounds there cannot be a pileup of particles in CHII behind junction B. In the same way, we do not expect an x-dependent $n_{\rm II}(x)$ that decreases with x from junction A to B. Thus, $n_{\rm II}(x)$ should be macroscopically uniform in the bulk. We are then left with only one solution $n_{\rm II}(x) = K/(1+K)$. This solution is independent of the boundaries A and B, and is thus akin to the maximal current (MC) phase of TASEP. There is, however, a crucial difference: in an MC phase of a TASEP, the steady-state bulk density reaches its maximum value of 1/2. However, with $n_{\rm II} = K/(1+K)$, the steady-state bulk density in CHII is *always* less than $1/2$ (with $K < 1$).

We therefore call it the *generalized MC* (GMC) phase [16]; see also Ref. [8] for analogous results in a similar open system. Now consider CHI: since the bulk steady-state density in CHII is $K/(1+K) = n_0$, the average steady-state density in CHI must also be $K/(1+K)$, in order to have n_0 as the mean density in the whole system. Notice that a uniform $n_{\rm I}(x) = n_0$ does solve (7) above. However, this solution is not admissible, as it manifestly violates current conservations at A and B. Thus, CHI can only admit macroscopically nonuniform density profiles in its NESS. If there are spatially varying LD phases in CHI (monotonically rising from B to A, remaining less than 1/2 everywhere), the current conservation at either junction A or B will be violated. This rules out a spatially varying LD phase in CHI. Clearly then, an analogous HD phase in CHI is also ruled out. Therefore, on physical grounds one part of the solution for $n_{\rm I}(x)$ should be $<1/2$ (near junction B) and another part $>1/2$ (near A) to maintain current conservation at both A and B; see

Eqs. (10) and (11) below. This leaves us with two possibilities: (a) the two parts of the solutions match smoothly with the bulk solution $n_{\rm I}(x) = n_0$, *without* any density discontinuity (CDP solution), or (b) the two parts *do not* meet with the bulk solution, leading to a density discontinuity (SP solution), as discussed below. These arguments are used below to analyze the phases in the model.

1. Phase diagrams and density profiles with an extended defect

As pointed out in the previous section, CHII is always in the GMC phase, with $n_{\rm II}(x) = n_0$ in the bulk. Since a pure LD (hence an HD) phase is ruled out in CHI, it should only have macroscopically inhomogeneous densities. This means there are no boundary layers in CHI at the junctions A and B. Then, applying the current conservation as given by Eq. (1), we get

$$n_{\rm I}(0) = \alpha_1 = \frac{1}{2}\left[1 - \frac{1}{1+K}\sqrt{(1+K)^2 - 4pK}\right] < \frac{K}{1+K} \tag{10}$$

and

$$n_{\rm I}(l) = \alpha_2 = \frac{1}{2}\left[1 + \frac{1}{1+K}\sqrt{(1+K)^2 - 4pK}\right] > \frac{1}{2}. \tag{11}$$

We also obtain the general solution to Eq. (7),

$$\frac{1}{a}\left[2n_{\rm I}(x) - \left(1 + \frac{2b}{a}\right)\ln|an_{\rm I}(x) + b|\right] = x + C, \tag{12}$$

where $a = \Omega(1+K)$ and $b = -\Omega K$. The constant of integration, C, is to be determined appropriately by using either the boundary conditions (10) or (11), yielding generally two different solutions. Defining $n_{\rm IB}(x)$ and $n_{\rm IA}(x)$ as the solutions of Eq. (7) corresponding to the boundary conditions (10) and (11), respectively, we find

$$2[n_{\rm IB}(x) - \alpha_1] - \left(1 + \frac{2b}{a}\right)\ln\left|\frac{an_{\rm IB}(x) + b}{a\alpha_1 + b}\right| = ax \tag{13}$$

and

$$2[n_{\rm IA}(x) - \alpha_2] - \left(1 + \frac{2b}{a}\right)\ln\left|\frac{an_{\rm IA}(x) + b}{a\alpha_2 + b}\right| = a(x - l). \tag{14}$$

Given the physical expectation that $n_{\rm I}(x)$ cannot decrease as x rises, we identify two points x_α and x_β, at which $n_{\rm IB}(x)$ and $n_{\rm IA}(x)$, respectively, meet with the bulk solution $n_{\rm I}(x) = n_0$. Defining $j_{\rm IB}(x)$ and $j_{\rm IA}(x)$ as the spatially varying currents corresponding to the densities $n_{\rm IB}(x)$ and $n_{\rm IA}(x)$, respectively: $j_{\rm IB}(x) = n_{\rm IB}(x)[1 - n_{\rm IB}(x)]$, $j_{\rm IA}(x) = n_{\rm IA}(x)[1 - n_{\rm IA}(x)]$, and $j_0(x) = n_0(1 - n_0)$, x_α and x_β may be obtained from $j_{\rm IB}(x) = j_0$ and $j_{\rm IA}(x) = j_0$. As in Ref. [14], three different scenarios are possible:

(i) *Continuous density phase* (CDP) corresponding to $x_\alpha < x_\beta$: $n_{\rm I}(x)$ rises from $n_{\rm I}(x = 0)$ to reach $n_{\rm I}(x) = n_0$ at x_α, and then rises again from x_β to reach $n_{\rm I}(x) = n_{\rm I}(x = l)$. Ignoring boundary layers, $n_{\rm II}(x) = n_0$, i.e., the GMC phase for CHII ensues. See Fig. 2 for a representative plot with CDP for $n_{\rm I}(x)$, where results from MFT and MCS studies are plotted together; good agreement between the MFT and MCS results are evident. Enumeration of x_α and x_β from MFT is shown in the inset.

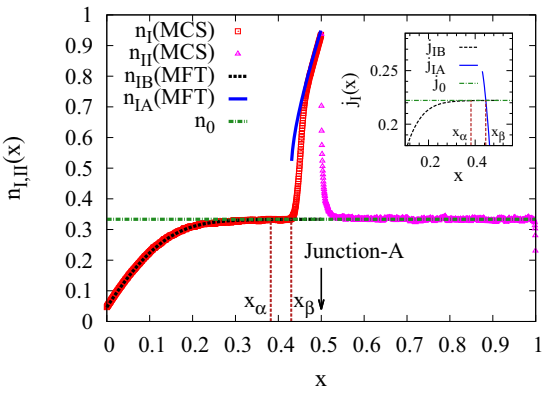

FIG. 2. Plots of the density profiles in CDP ($K = 0.5$, $p = 0.2$, $\Omega = 4.5$, $l = 1/2$, $N = 2000$). Mean-field solutions $n_{\rm IB}(x)$ (black dotted line), $n_{\rm IA}(x)$ (blue solid line), and the corresponding MCS results $n_{\rm I}(x)$ (red squares) are shown. MCS results for $n_{\rm II}(x)$ are shown with magenta triangles; x_α and x_β are extracted from MCS data (see the text). n_0 (green dotted line) is the average density of the system. Inset: mean-field values of the currents $j_{\rm IB}(x)$, $j_{\rm IA}(x)$, and $j_0(x)$ are plotted; x_α and x_β are extracted (see the text), which match well with their corresponding MCS results.

While with $K = 1$, $n_{\rm I}(x)$ takes a very simple form as a function of x [14], for $K \neq 1$ its functional form is more complex. Nonetheless, from the structures of Eqs. (7), (13), and (14), we can make the following general observations. (a) In general, $n_{\rm IA} > n_0 = n_{\rm II}(x) > n_{\rm IB}$; (b) the slopes $\partial n_{\rm IB,A}/\partial x \to 0$ as $n_{\rm IB,A}(x) \to K/(1+K)$ at some points in the bulk; (c) with $K < 1$, $\partial n_{\rm IB}(x)/\partial x$ never diverges, whereas $\partial n_{\rm IA}(x)/\partial x$ diverges as $n_{\rm I}(x) \to 1/2$. Thus broadly, the slope $n_{\rm IA}(x)$ should be *steeper* than that of $n_{\rm IB}(x)$ [15]. It is also clear that $n_{\rm IA}(x)$ starts from $n_{\rm IA}(x = x_\beta) = n_0 < 1/2$ for $K < 1$ to rise to (11) that is larger than $1/2$. Thus, $n_{\rm IA}(x)$ is a combination of LD-HD phases. For $K = 1$, $n_{\rm IA}(x)$ is necessarily more than $1/2$, and hence fully HD. (d) Lastly, $n_{\rm I}(x)$ starts from LD (i.e., LD near junction B) and ends in HD (i.e., HD near junction A) always. These are consistent with our observations from MCS results; see Fig. 2.

(ii) *Shock phase* (SP) corresponding to $x_\alpha > x_\beta$ [14]. There is no intervening flat portion in $n_{\rm I}(x)$. Instead, $n_{\rm I}(x)$ discontinuously changes from its value $n_{\rm IB}$ to $n_{\rm IA}$ at $x = x_w$, yielding a density shock or a localized domain wall (LDW) at $x = x_w$. The condition $j_{\rm IB}(x_w) = j_{\rm IA}(x_w)$ yields x_w. Density $n_{\rm II}(x)$ remains at its GMC phase, i.e., $n_{\rm II}(x) = n_0$, just like the CDP. See Fig. 3 for a representative plot for SP of $n_{\rm I}(x)$. Again, the agreement between MFT and MCS results is close. In the inset, enumeration of x_w from MFT is shown.

(iii) The borderline case with $x_\alpha = x_\beta$: this corresponds to $j_{\rm IB}(x) = j_{\rm IA}(x) = j_0$ at $x = x_\alpha = x_\beta$. A representative profile of $n_{\rm I}(x)$ with $x_\alpha = x_\beta$, i.e., at the boundary between SP and CDP, is shown in Fig. 4; the inset shows a plot of the numerical evaluation of $x_\alpha = x_\beta$ from the MFT. Unlike for $K = 1$, for which the density profiles at $x_\alpha = x_\beta$ are linear [14] [because the factor $1 + \frac{2b}{a}$ appearing in Eq. (12) becomes zero for $K = 1$], for $K < 1$ the same factor is not zero and hence we do not get a linear density profile at the borderline case separating the CDP and SP regions. It may be noted that our above results

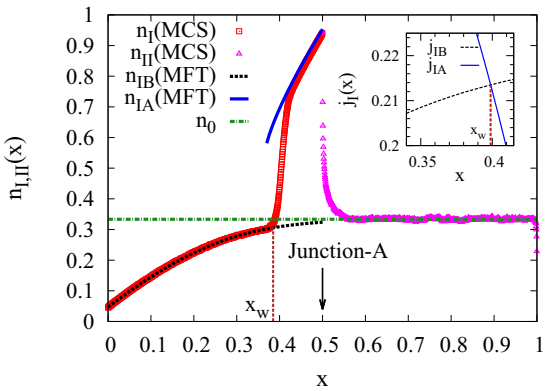

FIG. 3. Plots of the density profiles in SP ($K = 0.5$, $p = 0.2$, $\Omega = 2.25$, $l = 1/2$, $N = 2000$). Mean-field solutions $n_{\rm IB}(x)$ (black dotted line), $n_{\rm IA}(x)$ (blue solid line), and the corresponding MCS results $n_{\rm I}(x)$ (red squares) are shown. MCS results for $n_{\rm II}(x)$ are shown with magenta triangles; x_w is extracted from MCS data (see the text). n_0 (green dotted line) is the average density of the system. Inset: mean-field values of the currents $j_{\rm IB}(x)$ and $j_{\rm IA}(x)$ are plotted; x_w has been extracted (see the text), which match well with their corresponding MCS results.

hold well for all l, $0 < l < 1$; we have reported here the results only for $l = 1/2$.

In Figs. 5 and 6, the phase diagrams for $l = 1/2$ in the Ω-p plane for $K = 0.5$ and 0.2, respectively, as obtained from our MCS and MFT approaches, are shown. Unsurprisingly, there are only two phases—CDP and SP—in both of them. The phase boundary between CDP and SP is determined from the condition $x_\alpha = x_\beta$ (see above). Similar to Ref. [14], the MCS and MFT results mutually agree qualitatively as well as quantitatively. The phase diagrams in Figs. 5 and 6 are qualitatively similar to each other, and they are also similar to the corresponding phase diagram for $K = 1$ in Ref. [14].

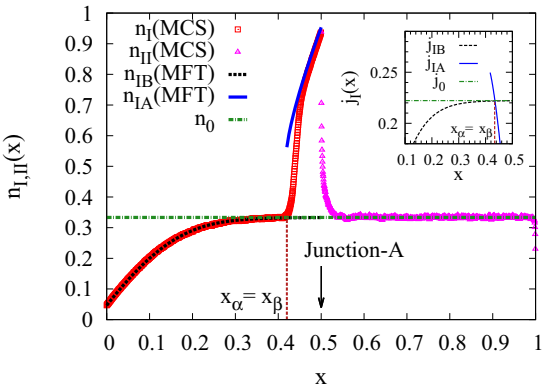

FIG. 4. Plots of the density profiles in the borderline case ($K = 0.5$, $p = 0.2$, $\Omega = 3.75$, $l = 1/2$, $N = 2000$). Mean-field solutions $n_{\rm IB}(x)$ (black dotted line), $n_{\rm IA}(x)$ (blue solid line), and the corresponding MCS results $n_{\rm I}(x)$ (red squares) are shown. MCS results for $n_{\rm II}(x)$ are shown with magenta triangles; x_α and x_β are extracted from MCS data (see the text). n_0 (green dotted line) is the average density of the system. Inset: mean-field values of the currents $j_{\rm IB}(x)$, $j_{\rm IA}(x)$, and $j_0(x)$ are plotted; x_α and x_β are extracted (see the text), which match well with their corresponding MCS results.

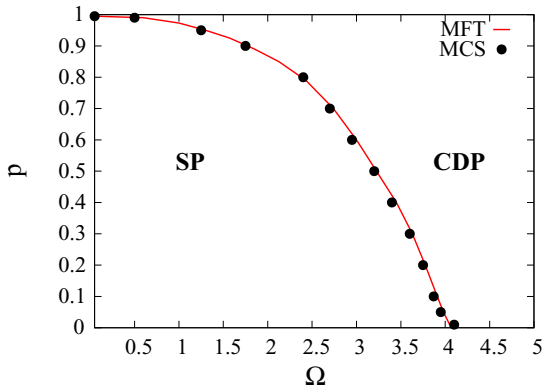

FIG. 5. Phase diagram in the Ω-p plane for extended defects, with $K = 0.5$: mean-field result (red continuous line) and MCS results (black circles) are shown, which agree well. Here $l = 1/2$ and $N = 1000$.

Still, Figs. 5 and 6 do not match quantitatively, nor do they agree quantitatively with the corresponding phase diagram for $K = 1$ in Ref. [14].

The region occupied by SP in Fig. 6 is noticeably larger than in Fig. 5, which in turn is larger than the two-phase region for $K = 1$; see Ref. [14]. This trend may be explained in simple terms. From Eqs. (10) and (11), it is clear that for small K, the jump in the values of $n_{\rm I}(x)$ across the extended defect is large. On the other hand, $\partial n_{\rm I}(x)/\partial x$ is clearly controlled by the factor $\Omega(1 + K)$; see Eq. (7). Now in order for the CDP to exist, $n_{\rm I}(x)$ must rise (fall) sharply enough from its value α_1 at $x = 0$ (α_2 at $x = l$) to match with $n_0 = K/(1 + K)$ in the bulk. Since $\partial n_{\rm I}(x)/\partial x$ is smaller for smaller K for a given Ω, a larger Ω is clearly needed with smaller K to ensure CDP. This explains why for $K = 0.2$ the CDP requires a higher Ω than for $K = 0.5$, which in turn has a higher-Ω threshold than that for three-phase coexistence for $K = 1$ [14].

The changes in the phase diagrams given in Figs. 5 and 6 with variation in K are also reflected in the corresponding plots

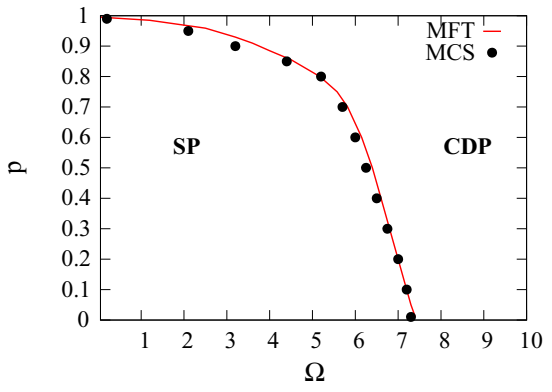

FIG. 6. Phase diagram in the Ω-p plane for extended defects, with $K = 0.2$: mean-field result (red continuous line) and MCS results (black circles) are shown, which agree well. Note that while Fig. 6 is quantitatively different from Fig. 5, the phase diagrams are qualitatively similar as they separate the same phases from each other. Here $l = 1/2$ and $N = 1000$.

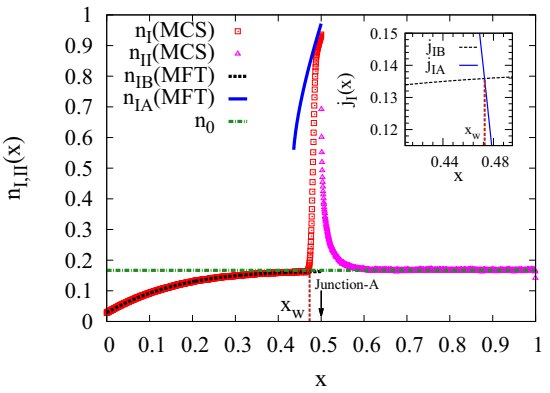

FIG. 7. Plots of the density profiles in SP ($K = 0.2$, $p = 0.2$, $\Omega = 4.5$, $l = 1/2$, $N = 2000$). Mean-field solutions $n_{\rm IB}(x)$ (black dotted line), $n_{\rm IA}(x)$ (blue solid line), and the corresponding MCS results $n_{\rm I}(x)$ (red squares) are shown. MCS results for $n_{\rm II}(x)$ are shown with magenta triangles; x_α and x_β are extracted from MCS data (see the text). n_0 (green dotted line) is the average density of the system. Inset: mean-field values of the currents $j_{\rm IB}(x)$, $j_{\rm IA}(x)$, and $j_0(x)$ are plotted; x_α and x_β are extracted (see the text), which match well with their corresponding MCS results.

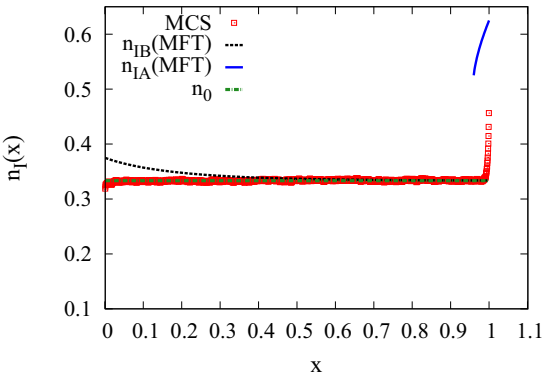

FIG. 8. Plots of the density profiles in the LD region for a point defect located at $x = 1$ ($K = 0.5$, $p = 0.6$, $\Omega = 1.0$, $N = 2000$). Mean-field solutions $n_{\rm IB}(x)$ (black dotted line), $n_{\rm IA}(x)$ (blue solid line), and the corresponding MCS results $n_{\rm I}(x)$ (red squares) are shown. n_0 (green dotted line) is the average density of the system. We have extended the x axis up to $x = 1.1$ to resolve the peak at $x = 1$ (the location of the point defect) properly.

of $n_{\rm I}(x)$ versus x. For instance, compare Fig. 2 ($K = 0.5$) with Fig. 7 ($K = 0.2$). Clearly, as K is reduced, a CDP density profile for $n_{\rm I}(x)$ gives way to a SP density profile. This is consistent with the trends observed in the above two phase diagrams.

In Table I, we compare the mean density in the NESS of the whole system as obtained from MCS with the predictions from MFT for an extended defect. Clearly, good agreement is found. This validates our MFT arguments elucidated above.

B. MF analysis and MCS results for a point defect

For a point defect, junctions A and B merge. As a result, the constraint from the constant bulk current in CHII on $j_{\rm I}(x) = n_{\rm I}(x)[1 - n_{\rm I}(x)]$ for an extended defect does not exist for a point defect. In fact, CHII effectively ceases to exist, and Eq. (8) no longer holds. The steady-state density $n_{\rm I}(x)$ of CHI now spans the whole system and satisfies Eq. (7),

$$[2n_{\rm I}(x) - 1]\frac{\partial n_{\rm I}(x)}{\partial x} - \Omega(1 + K)\left(n_{\rm I}(x) - \frac{K}{1 + K}\right) = 0. \tag{15}$$

We now argue that (15) allows for a spatially uniform steady-state density in CHI, with a localized peak at the location of the point defect. Evidently, (15) allows for a uniform solution $n_{\rm I}(x) = K/(1 + K) < 1/2$ ($K < 1$), in addition to the space-dependent solutions, akin to the solutions of $n_{\rm I}(x)$ in the extended defect case, in the NESS of the model. As argued in Refs. [10,12], for a sufficiently low average density, the effect of the point defect is confined to creating a localized peak (or a dip) that has a vanishing width in the thermodynamic limit in an otherwise homogeneous density profile. In other words, the bulk density should be uniform for sufficiently low average density. For a ring geometry, this implies $n_{\rm I}(x) = K/(1 + K)$, with $n_{\rm I}(x) = n_0 + h$ having a localized peak of height $h = n_0(1 - p)/p$ at the location of the point defect [10,12]. This is consistent with our discussions above. See Fig. 8 for a representative plot of $n_{\rm I}(x)$ as a function of x in the LD phase. As n_0 rises (i.e., K rises), or the defect strength rises (i.e., p decreases), eventually this picture breaks down and the point defect then leads to macroscopically nonuniform density profiles. Following the logic outlined in Refs. [10,12], we find the threshold of inhomogeneous phases to be

$$\frac{K}{1 + K} = \frac{p}{1 + p} \Rightarrow K = p. \tag{16}$$

Therefore, as K exceeds p, spatially nonuniform density profiles are to be formed in the NESS.

For $K > p$, the spatially varying solutions of $n_{\rm I}(x)$ may be analyzed as before. Without any loss of generality, we assume that the site with the defect is located at $x = 1$. Assuming that the particles hop anticlockwise as before, one expects that $n(1 - \epsilon) > n(\epsilon)$, where $\epsilon \to 0$. Let ρ_L and ρ_R be the densities at the left and right of $x = 1$. Now assume phase coexistence for $n_{\rm I}(x)$ in the NESS, i.e., no boundary layers at $x = 1$. Applying the current conservation at $x = 1$, we get

$$\rho_L(1 - \rho_L) = p\rho_R(1 - \rho_L) = \rho_R(1 - \rho_R). \tag{17}$$

This gives $\rho_L = \frac{p}{1+p}$ and $\rho_R = \frac{1}{1+p}$. The CHI density is then obtained by using Eq. (7) along with the boundary conditions

$$n_{\rm I}(0) = \frac{p}{1 + p} \text{ and } n_{\rm I}(1) = \frac{1}{1 + p}. \tag{18}$$

TABLE I. A comparison of the average density value n_0 obtained from MCS and MFT for an extended defect. Here $\Omega = 2.5$ and $p = 0.5$, and $N = 2000$.

K	0.2	0.5	1.0
n_0 (MCS)	0.166 672	0.333 547	0.499 187
n_0 (MFT)	0.166 667	0.333 333	0.5

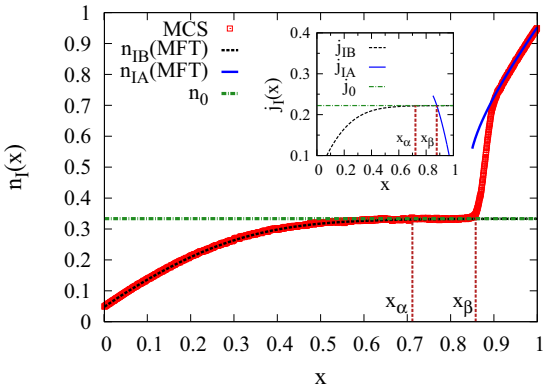

FIG. 9. Plots of the density profiles in the CDP ($K = 0.5$, $p = 0.05$, $\Omega = 2.0$, $N = 2000$). Mean-field solutions $n_{\rm IB}(x)$ (black dotted line), $n_{\rm IA}(x)$ (blue solid line), and the corresponding MCS results $n_{\rm I}(x)$ (red squares) are shown; x_w is extracted from MCS data (see the text). n_0 (green dotted line) is the average density of the system. Inset: mean-field values of the currents $j_{\rm IB}(x)$ and $j_{\rm IA}(x)$ are plotted; x_w has been extracted (see the text). Qualitative agreement with their corresponding MCS results is evident.

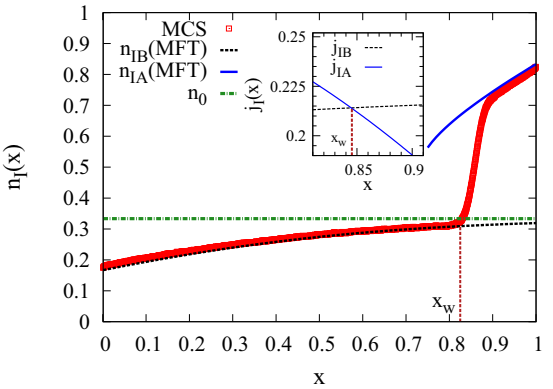

FIG. 10. Plots of the density profiles in the SP phase ($K = 0.5$, $p = 0.2$, $\Omega = 0.75$, $N = 2000$). Mean-field solutions $n_{\rm IB}(x)$ (black dotted line), $n_{\rm IA}(x)$ (blue solid line), and the corresponding MCS results $n_{\rm I}(x)$ (red squares) are shown; x_w is extracted from MCS data (see the text). n_0 (green dotted line) is the average density of the system. Inset: mean-field values of the currents $j_{\rm IB}(x)$ and $j_{\rm IA}(x)$ are plotted; x_w has been extracted (see the text). Qualitative agreement with their corresponding MCS results is evident.

As for the extended defect case, there are three different solutions: two spatially varying depending upon the boundary conditions (18), and a third bulk solution $n_{\rm I}(x) = K/(1+K) = n_0$ that is independent of x. The spatially varying solutions are

$$2\left(n_{\rm IB}(x) - \frac{p}{1+p}\right) - \left(1 + \frac{2b}{a}\right) \ln\left|\frac{an_{\rm IB}(x)+b}{\frac{ap}{1+p}+b}\right| = ax \tag{19}$$

and

$$2\left(n_{\rm IA}(x) - \frac{1}{1+p}\right) - \left(1 + \frac{2b}{a}\right) \ln\left|\frac{an_{\rm IA}(x)+b}{\frac{a}{1+p}+b}\right| = a(x-1). \tag{20}$$

Again as in CDP with an extended defect, we can define x_α and x_β from the conditions $n_{\rm IB}(x_\alpha) = n_0$ and $n_{\rm IA}(x_\beta) = n_0$. Equivalently, defining currents $j_{\rm IA}(x) = n_{\rm IA}(x)[1 - n_{\rm IA}(x)]$, $j_{\rm IB}(x) = n_{\rm IB}(x)[1 - n_{\rm IB}(x)]$, and $j_0(x) = n_0(1 - n_0)$, x_α and x_β are obtained from $j_{\rm IB}(x_\alpha) = j_0$ and $j_{\rm IA}(x_\beta) = j_0$, respectively. Similar to the extended defect case (see also Ref. [14]), three distinct cases are possible:

(i) CDP for $x_\alpha < x_\beta$: $n_{\rm I}(x)$ is qualitatively similar to its analog for the extended defect case. A representative plot of $n_{\rm I}(x)$ in its CDP as a function of x is shown in Fig. 9.

(ii) SP with $x_\alpha > x_\beta$ yielding an LDW at $x = x_w$. A representative plot of $n_{\rm I}(x)$ in its SP as a function of x with an LDW at $x = x_w$ is shown in Fig. 10.

(iii) The borderline case between CDP and SP given by $x_\alpha = x_\beta$; see Fig. 11.

To find out the phase boundary between the CDP and SP regions, we proceed in the same way as in case of extended defects, that is, we find out p and Ω values for which $x_\alpha = x_\beta$. For $K < p$, the system is in a spatially homogeneous LD phase. The phase diagram for the case of a point defect showing the three distinct phase regions is shown in Figs. 12 and 13.

Notice that the extent of the LD phase in Fig. 13 is distinctly larger than that in Fig. 12. This is consistent with the fact that the boundary between LD and the spatially inhomogeneous phases (SP or CDP) in MFT is given by $p = K$ (in agreement with MCS results), which clearly yields a larger LD phase in the Ω-p plane for a lower K. Next, consider the relative preponderance of the SP over the CDP in Fig. 13 in comparison with Fig. 12. Unlike the case with an extended defect, the jump in an inhomogeneous $n_{\rm I}(x)$ at the point defect depends only on p, and not on K, regardless of SP or CDP. Nonetheless, as discussed above, the slope $\partial n_{\rm I}(x)/\partial x$ in NESS is still controlled by $\Omega(1+K)$. Hence, for reasons similar to those for an extended defect, in a Ω-p phase diagram the CDP starts

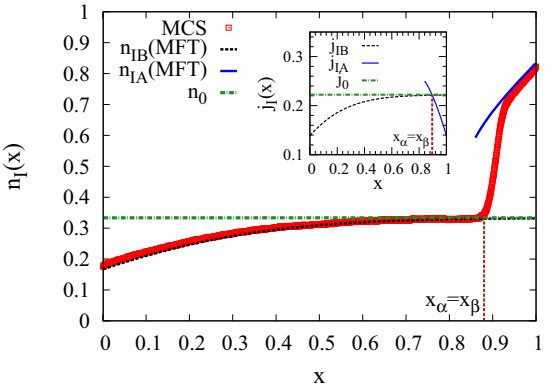

FIG. 11. Plots of the density profiles in the borderline case for a point defect located at $x = 1$ ($K = 0.5$, $p = 0.2$, $\Omega = 1.25$, $N = 2000$). Mean-field solutions $n_{\rm IB}(x)$ (black dotted line), $n_{\rm IA}(x)$ (blue solid line), and the corresponding MCS results $n_{\rm I}(x)$ (red squares) are shown; x_α and x_β are extracted from MCS data (see the text). n_0 (green dotted line) is the average density of the system. Inset: mean-field values of the currents $j_{\rm IB}(x)$, $j_{\rm IA}(x)$, and $j_0(x)$ are plotted; x_α and x_β are extracted (see the text), which match well with their corresponding MCS results.

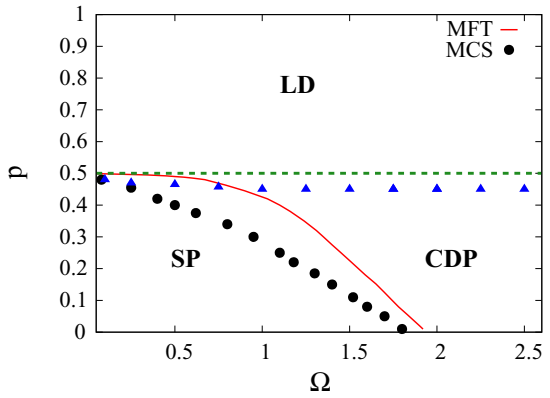

FIG. 12. Phase diagram in the Ω-p plane for a point defect located at $x = 1$, with $K = 0.5$: mean-field results (red solid line) and the MCS results are shown. The green dotted horizontal line, separating the LD phase from other phase regions, is obtained from MFT and satisfies the equation $p = K$. The corresponding MCS data points are represented by the blue triangles. Here $N = 1000$.

for a higher Ω with a lower K. For $K = 1$, there is no LD phase even for a point defect. For a putative LD phase, one must have $p > K$; for $K = 1$ this condition rules out an LD phase.

The quantitative dissimilarities between the phase diagram in Ref. [14] for a point defect and the inhomogeneous parts of those in Figs. 12 and 13 may be explained following the logic outlined in the discussions on the phase diagrams for an extended defect above. These differences can lead to qualitative differences in the density profiles in the NESS. For instance, compare Fig. 9 ($K = 0.5$) and Fig. 14 ($K = 0.2$) to observe that the CDP density profile for $K = 0.5$ has become a SP density profile for $K = 0.2$. This trend is similar to what one finds for extended defects.

In Table II, we compare the values of the mean densities obtained from MCS with the corresponding MFT results for

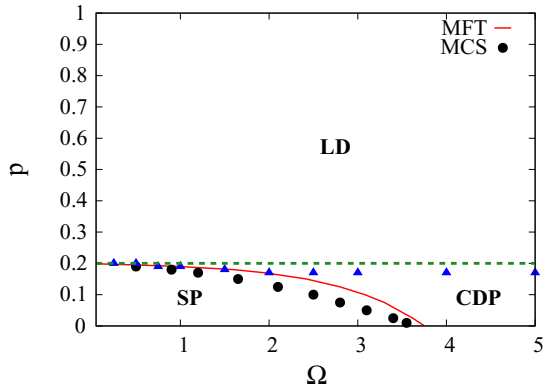

FIG. 13. Phase diagram in the Ω-p plane for a point defect located at $x = 1$, with $K = 0.2$: mean-field results (red solid line) and the MCS results are shown. The green dotted horizontal line, separating the LD phase from other phase regions, is obtained from MFT and satisfies the equation $p = K$. The corresponding MCS data points are represented by the blue triangles. Note that a lower value of K corresponds to a lower attachment rate, and hence the LD profile occupies a bigger region in the phase diagram than it does for a higher value of K (see Fig. 12). Here $N = 1000$.

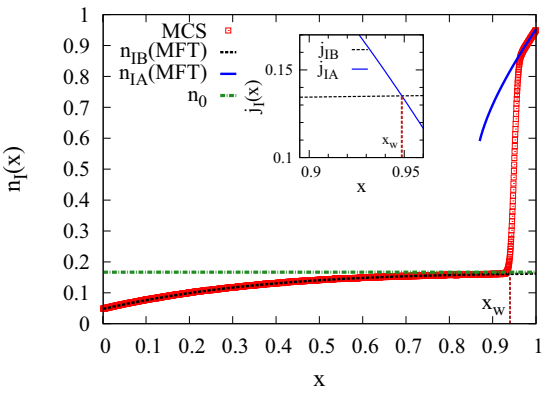

FIG. 14. Plots of the density profiles in the SP for a point defect located at $x = 1$ ($K = 0.2$, $p = 0.05$, Ω = 2.0, $N = 2000$). Mean-field solutions $n_{\rm IB}(x)$ (black dotted line), $n_{\rm IA}(x)$ (blue solid line), and the corresponding MCS results $n_{\rm I}(x)$ (red squares) are shown; x_α and x_β are extracted from MCS data (see the text). n_0 (green dotted line) is the average density of the system. Inset: mean-field values of the currents $j_{\rm IB}(x)$, $j_{\rm IA}(x)$, and $j_0(x)$ are plotted; x_α and x_β are extracted (see the text), which match well with their corresponding MCS results.

different values of K. Again, similar to the extended defect case, there is good quantitative agreement between the two, lending credence to our MFT results.

IV. COMPARISON WITH $K = 1$

Having discussed the studies with $K \neq 1$ for both extended and point defects, let us now compare and contrast the results here with the corresponding results for $K = 1$. There are some similarities and some significant differences.

For instance, with an extended defect, the model yields nonuniform densities in the faster segment for both $K = 1$ and $K \neq 1$. However, for $K = 1$, the density profiles in the faster part of the system consist of three clear segments, all of which are straight lines, belonging to the LD, MC, and HD phases. In contrast, with $K \neq 1$, such a clear classification fails; additionally, the density profiles are *not* straight lines. Furthermore, the slower part of the system with an extended defect is in the GMC phase, with a density generically different from 1/2 in the bulk for $K \neq 1$, whereas for $K = 1$, the corresponding density is in the usual MC phase with a bulk value of 1/2. The distinctiveness of $K \neq 1$ manifests more starkly for a point defect: it is now possible to have a pure LD phase, which is ruled out for $K = 1$. In addition, the spatially nonuniform density profiles with a point defect for $K \neq 1$ can no longer be characterized as simple combinations of LD, MC, and HD phases, unlike for $K = 1$.

TABLE II. Table comparing the average density value n_0 obtained from MCS and MFT for a point defect. Here Ω = 1.0, $p = 0.5$ and $N = 2000$.

K	0.2	0.5	1.0
n_0 (MCS)	0.166 915	0.333 366	0.499 587
n_0 (MFT)	0.166 667	0.333 333	0.5

V. SUMMARY AND OUTLOOK

In this work, we have studied an asymmetric exclusion process in an inhomogeneous ring with particle-nonconserving LK dynamics. The attachment and detachment rates of LK are generally assumed to be unequal. We have considered both extended and point defects. The MFT analysis is done by assuming the system to be a combination of two TASEP channels CHI (of hopping rate 1) and CHII (of hopping rate $p < 1$) of unequal hopping rates, which are joined together at both the ends. For a point defect, CHII shrinks to a point. Our MFT analysis, backed up by extensive MCS studies, clearly reveals that with an extended defect, $n_{\rm II} = K/(1+K)$ in the bulk of CHII, a constant that is independent of $p(< 1)$ (i.e., independent of the boundaries or junctions at A and B). In analogy with the MC phase of an open TASEP, we call this the GMC phase. In contrast, CHI is found in either CDP or SP. Unsurprisingly, CDP is favored for larger Ω, whereas SP prevails for smaller Ω for fixed p, K, as in Ref. [14]. For a point defect, for which CHII shrinks to a point, for $K < p$, $n_{\rm I}(x)$ is found in a uniform phase, unlike an extended defect. The variations in the phase diagrams with K are explained in simple physical terms. As in Ref. [14], the quantitative agreement between the MCS and MFT results for an extended defect is very high, as is evident in the corresponding phase diagram; see Figs. 5 and 6. In contrast, the agreement for the point defect case is weaker, particularly for small Ω. The physical reasons behind these discrepancies are expected to be the same as that elaborated in Ref. [14].

Our results clearly bring out the relevance of the ring or closed geometry of the system in the presence of LK with unequal attachment and detachment rates. The results here as well as those in Ref. [14] clearly establish how the ring geometry (or the lack of independent entry and exit events) restricts the possible phases in these models, in comparison with the results on the corresponding open system; see Refs. [8,10]. It would be interesting to numerically study the crossover between the extended and point defect cases by varying N while keeping the length of the slower segment unchanged. As an alternative to our simple MFT, it should be interesting to extend the boundary-layer formalism developed in Ref. [17] for the present problem. The simplicity of our model limits direct applications of our results to practical or experimental situations. Nonetheless, our above results in the context of vehicular traffic along a circular track, or railway movements in series along a closed railway loop line with possibilities of new carriages joining or existing carriages going off the loop track in the presence of constrictions (regions of slow passages due to, e.g., accidents or damages in the tracks), or ribosome translocations along mRNA loops with defects and random attachment and detachment, clearly demonstrate that for extended defects, the steady-state densities are generally inhomogeneous, whereas for a point defect, globally uniform densities are possible for a sufficiently low average density. We hope that experiments on ribosomes using ribosome profiling techniques [18] and numerical simulations of more detailed traffic models will qualitatively validate our results.

ACKNOWLEDGMENTS

S.M. acknowledges the financial support from the Council of Scientific and Industrial Research, India [Grant No. 09/489(0096)/2013-EMR-I]. T.B. and A.B. gratefully acknowledge partial financial support from Alexander von Humboldt Stiftung, Germany under the Research Group Linkage Programme (2016).

[1] J. Ziman, *Models of Disorder: The Theoretical Physics of Homogeneously Disordered Systems* (Cambridge University Press, Cambridge, MA, 1979); R. Stinchcombe, *Dilute Magnetism*, Vol. 7 of *Phase Transition and Critical Phenomena* (Academic, New York, 1983).

[2] R. Stinchcombe, J. Phys.: Condens. Matter **14**, 1473 (2002).

[3] D. Chowdhury, L. Santen, and A. Schadschneider, Phys. Rep. **329**, 199 (2000); D. Helbing, Rev. Mod. Phys. **73**, 1067 (2001); T. Chou, K. Mallick, and R. K. P. Zia, Rep. Prog. Phys. **74**, 116601 (2011).

[4] I. Kosztin and K. Schulten, Phys. Rev. Lett. **93**, 238102 (2004).

[5] C. T. MacDonald, J. H. Gibbs, and A. C. Pipkin, Biopolymers **6**, 1 (1968); R. Lipowsky, S. Klumpp, and T. M. Nieuwenhuizen, Phys. Rev. Lett. **87**, 108101 (2001).

[6] J. Kärger and D. Ruthven, *Diffusion in Zeolites and Other Microporous Solids* (Wiley, New York, 1992)

[7] B. Alberts *et al.*, *Molecular Biology of the Cell* (Garland Science, New York, 2002).

[8] A. Parmeggiani, T. Franosch, and E. Frey, Phys. Rev. E **70**, 046101 (2004).

[9] J. J. Dong, B. Schmittmann, and R. K. P. Zia, J. Stat. Phys. **128**, 21 (2007); P. Greulich and A. Schadschneider, Physica A **387**, 1972 (2008); R. K. P. Zia, J. J. Dong, and B. Schmittmann, J. Stat. Phys. **144**, 405 (2011); J. S. Nossan, J. Phys. A **46**, 315001 (2013).

[10] P. Pierobon, M. Mobilia, R. Kouyos, and E. Frey, Phys. Rev. E **74**, 031906 (2006).

[11] G. Tripathy and M. Barma, Phys. Rev. E **58**, 1911 (1998)

[12] N. Sarkar and A. Basu, Phys. Rev. E **90**, 022109 (2014).

[13] T. Banerjee, N. Sarkar, and A. Basu, J. Stat. Mech.: Theor. Exp. (2015) P01024.

[14] T. Banerjee, A. K. Chandra, and A. Basu, Phys. Rev. E **92**, 022121 (2015).

[15] Notice that this condition cannot be used for $K = 1$ as in Ref. [14], where the factor $2n_{\rm I}(x) - 1$ vanishes as $n_{\rm I}(x) \to 1/2$, making the slope $\partial n_{\rm I}(x)/\partial x$ indeterminate. This suggests a discontinuity in the slope, unlike here, where the slope changes continuously. This is borne out by our MCS studies as well.

[16] For $K > 1$, $n_{\rm II}(x) = K/(1+K) > 1/2$ always.

[17] S. Mukerjee and S. M. Bhattacharjee, J. Phys. A **38**, L285 (2005); S. Mukherji and V. Mishra, Phys. Rev. E **74**, 011116 (2006); S. M. Bhattacharjee, J. Phys. A **40**, 1703 (2007); S. Mukherji, Phys. Rev. E **79**, 041140 (2009); **83**, 031129 (2011); A. K. Gupta and I. Dhiman, *ibid.* **89**, 022131 (2014).

[18] Y. Arava *et al.*, Nucl. Acids Res. **33**, 2421 (2005); N. T. Ingolia, S. Ghaemmaghami, J. R. S. Newman, and J. S. Weissman, Science **324**, 218 (2009); H. Guo *et al.*, Nature (London) **466**, 835 (2010).